

Europa's Sodium Atmosphere: An Ocean Source?

F. Leblanc

Service d'Aéronomie du CNRS, Verrières-Le-Buisson, France; and University of Virginia, Charlottesville, Virginia

R. E. Johnson

University of Virginia, Charlottesville, Virginia

and

M. E. Brown

California Institute of Technology, Pasadena, California

Received January 29, 2001; revised May 24, 2002

Sputtering and decomposition of Europa's surface by energetic ions and electrons produce an atmosphere. Here we use a 3D Monte Carlo simulation, including collisions with the background O₂ atmosphere, to describe recent measurements of the sodium component of the atmosphere. By constraining the model with the observational data, we attempt to reconstruct the source processes, the energy distribution, and the flux of the ejected sodium. We confirm that electronic sputtering from ice-rich regions dominates the ejecta and that Europa loses between 5 and 10×10^6 Na cm⁻² s⁻¹. This is about one order of magnitude more sodium than that implanted from the jovian magnetosphere. © 2002 Elsevier Science (USA)

Key Words: Europa; surface; satellite; atmosphere; composition.

1. INTRODUCTION

Jupiter's moon Europa continues to be one of the most interesting objects in the Solar System because of its geologically young surface (e.g., Pappalardo *et al.* 1999), a possible "salty" subsurface ocean (e.g., Kivelson *et al.* 2000), and the existence of a tenuous atmosphere (e.g., Hall *et al.* 1995). In addition, Europa's surface and atmosphere are in a rough chemical steady state with the external radiation field (Carlson *et al.* 1999, Cooper *et al.* 2001, Paranicas *et al.* 2000). Therefore, studying the origin and evolution of its thin atmosphere can lead to an understanding of the surface composition. Since Europa's surface is young, this understanding could, in principle, lead to information on the subsurface material (Johnson *et al.* 1998).

As predicted from laboratory measurements (Johnson 1990), the decomposition of water ice due to the charged-particle irradiation of the surface produces an O₂ atmosphere with a surface density $\sim 10^8$ cm⁻³ and a column density $\sim 10^{15}$ cm⁻² (Johnson *et al.* 1982, Hall *et al.* 1995, Ip *et al.* 1998, Saur *et al.* 1998). A much thinner atmosphere of Na has also been measured (Brown

and Hill 1996), with a column density of sodium $\sim 10^{10}$ cm⁻² and an even smaller potassium atmosphere (Brown 2001). The observation of a potassium-to-sodium ratio different from that at Io and a recent analysis of the sodium observations (Johnson 2000, Johnson *et al.* 2002) both suggest that the observed sodium is not due to the implantation of sodium ions from the jovian plasma torus. Therefore, the observed sodium may be endogenic. With the upward revision of the Brown and Hill (1996) sodium column density by Brown (2002), both the surface density and the escape flux analyzed by Johnson (2000) should be increased, strengthening the argument for an endogenic source. A possible source is irradiation decomposition of a frozen ocean mineral, such as a hydrated salt (e.g., Na₂SO₄XH₂O; Na₂CO₃XH₂O) (Johnson 2001).

In this paper we reexamine the sodium cloud using a new set of observations (Brown 2002) and a much more detailed modeling of the ejected sodium atoms. Whereas Brown & Hill (1996) in their discovery paper provided a profile of the atmospheric column density perpendicular to the orbit plane, the new measurements give a number of averaged profiles of the column density along perpendicular and parallel directions. These data require that we consider the asymmetric character of the Na cloud due mainly to the combined effects of Europa and Jupiter. For this purpose, we use a 3D Monte Carlo model in which the sodium atoms ejected from Europa's surface are followed. The atoms cross a thin O₂ atmosphere and move under the combined effect of the gravity fields of Jupiter and Europa. By adjusting the simulated cloud to the morphology observed by Brown (2002), we are able to estimate an ejected atom energy distribution and spatial distribution for the sputtered sodium. This allows us to more accurately quantify the nature of the sodium source.

Section 2 is a description of the observations (Section 2.1) and of the 3D Monte Carlo approach used in this paper (Sections 2.2 and 2.3). We compare the measurements and simulations leading

to a rough spatial and velocity distribution for the sputter source in Sections 3.1 and 3.2. In Section 3.3, we discuss the ultimate source of the observed Na. We confirm that it is much larger than the implantation source and is likely, therefore, to be endogenic. This is followed by a summary.

2. OBSERVATIONS AND MODEL OF THE SODIUM CLOUD

2.1. Observations

The observations used in this work have been obtained by Brown (2002) on 28 December 1999 during 3 h 30 min at the Keck telescope. The positions of Europa and Io at the start time of the measurements (separated in 6 sets of scans) are indicated in Table I. The size of the observing slit is 0.56 arcsec wide. Nine scans (set number 1) were first made along a north–south axis that is perpendicular to Europa’s orbital plane with the scans centered on Europa. Each scan corresponded to 4 min of integration. Eight scans along the east–west axis (set number 2) were then made with the 4-min scan again centered on Europa. Three scans (number 3) also along the east–west axis but at 10 R_E (Europa radii) to the north of Europa were then made each with 10 min of integration. This last set was then followed by three scans (number 4) along the east–west axis at 10 R_E to the south of Europa. Finally, four 15-min scans along the east–west axis were made, two (number 5) at 20 R_E north and two (number 6) at 20 R_E south. The observations shown in this paper are the averages of all the scans for each sequence of measurements. The overall calibration has been made from Jupiter’s disk. A conservative estimate of the overall calibration error is $\sim 20\%$ and is indicated in the figures presented in this paper. Point-to-point variation is small, as is shown. At the time of the measurements, Europa was at an average phase angle of 115° (see Table I). At the beginning of the measurements, Europa was at -4.7° magnetic latitude compared to Jupiter’s plasma torus centrifugal equator and at the end was at -2.9° after passing through a maximum around -9.6° . We started by finding the best fit to the observations ignoring the variation of Europa’s position inside Jupiter’s magnetosphere. That is, we consider that the jovian magnetospheric characteristics (the ion and electron densities) are constant at Europa’s orbit. We then discuss the variability.

TABLE I
28 December 1999, Keck Telescope (Brown 2002)

Set	Scans’ position	Time (UT)	System III (CML)	Europa phase	Io phase
1	N/S centered	4:28	260	109	347
2	E/W centered	5:16	288	112	353
3	E/W 10 R_E north	6:04	318	115	355
4	E/W 10 R_E south	6:37	337	117	4
5	E/W 20 R_E north	7:14	1	120	11
6	E/W 20 R_E south	7:45	19	122	15

Note. Time and position are for the start of each set of scans.

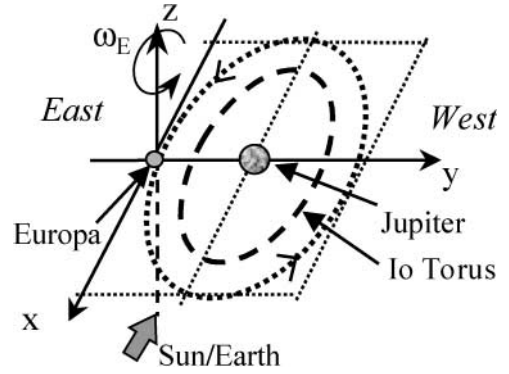


FIG. 1. Coordinate system used in the 3D Monte Carlo simulation for position shown for Europa. x , towards the sun; y , towards Jupiter; z , perpendicular to Europa orbital plane.

2.2. 3D Monte Carlo Model

A 3D Monte Carlo simulation is used to describe Europa’s sodium cloud. We assume in the following that the sodium is primarily sputtered as Na atoms with a small molecular component, NaX where X could be oxygen or sulfur (Wiens *et al.* 1997, Chrisey *et al.* 1988). Since a fraction of sputtered sodium returns to Europa’s surface and sodium ions are implanted in the surface, we assume, as did Johnson (2000), that sodium is sputtered from both icy and refractory regions by the energetic particle radiation. These source regions can result in different ejecta speed (Johnson *et al.* 2002) and spatial distributions at Europa’s surface.

Each particle that is ejected (sputtered) from the surface is followed along its trajectory in a coordinate system linked to Europa (Fig. 1). We assume that the motion of Europa around Jupiter is in the (xy) plane and the rotation vector, ω_E , of Europa around Jupiter and around itself is along the z -direction. The x -direction is in the direction of the motion of Europa towards the observer at the time of the observations (see Fig. 1). We suppose also that at the time of the observations, the solar flux direction is along the x -axis and then neglect the variations of the Na cloud emissions from 90° (the mean position of the cloud assumed in our simulation) to 115° in Europa geocentric phase angle (the mean position of Europa during the observations). Positive y is towards Jupiter. In this paper, the east–west direction is along the y -axis and the north–south direction is along the z -axis.

The motion of a particle sputtered from the surface of Europa is determined from the equation

$$m \left(\frac{d^2 r}{dt^2} \right)_E = F(r) + (a_E)_J + F_{cen}(r) + F_{cor}(r) + F(part/O_2), \quad (1)$$

where m is the mass of the particle and

- $(d^2 r/dt^2)_E$ is the acceleration of a particle of position vector r in the Europa coordinate system.

• $F(r)$ is the sum of all the forces in an inertial frame that act on the motion of this particle, $F(r) = F_J + F_E + F_{rad}$ with

$$\begin{aligned} F_J &= -m \frac{GM_J}{r'^3} r' \\ F_E &= -m \frac{GM_E}{r^3} r. \end{aligned} \quad (2)$$

F_J and F_E are the gravitational forces due to Jupiter and Europa. r' is the position vector of the particle in the Jupiter coordinate system. G is the gravitation constant, M_J is the mass of Jupiter, and M_E is the mass of Europa. Finally, F_{rad} is the solar radiation pressure which is calculated using the photon flux with respect to the wavelength provided by Brown and Yung (1976). This force generates an east–west asymmetry in Io’s sodium cloud (Smyth 1979, 1983; see also Smyth and Combi 1987). The photon flux is determined from the relative speed of each particle and the Sun, and the derived doppler shift determines the brightness of the Sun seen by the atom in the D1 and D2 absorption lines.

• $(a_E)_J$ is the acceleration of the coordinate system linked to Europa in Jupiter’s reference frame and is equal to the Jupiter gravitational force acting on Europa, $(a_E)_J = +[mGM_J/R_{EJ}^2]j$, where j is a direction vector from Europa towards Jupiter along y . R_{EJ} is the distance from Europa to Jupiter which is set to be equal to $9.4 R_J$ (Jupiter radii) or $427 R_E$.

• $F_{cor}(r)$ is the Coriolis force due to the rotation of Europa around Jupiter: $F_{cor}(r) = -2m\omega_E \times (dr/dt)_E$, where $(dr/dt)_E$ is the velocity of the particle with position vector r in the Europa coordinate system.

• $F_{cen}(r)$ is the centrifugal force acting on the particle and due to the rotation of Europa: $F_{cen}(r) = -m\omega_E \times (\omega_E \times r)$.

• $F(part/O_2)$ is the effective force due to the collisions of the particle with the O_2 molecules of Europa’s atmosphere. The characteristics of the O_2 atmosphere are from Saur *et al.* (1998). We use an atmospheric scale height equal to 135 km and a surface density of $4 \times 10^7 \text{ cm}^{-3}$, which roughly reproduces the $\sim 10^{15} \text{ cm}^{-2}$ column density suggested by Hall *et al.* (1995). Sputtered particles can collide with the O_2 . This is described as collisions between ejected Na or NaX (treated as a heavy atom) and O atoms, where the density of the oxygen atoms is twice that of O_2 . At each time step, in each cell of the domain of calculation, the number of collisions between the ejected particles and the representative O atoms of Europa’s atmosphere is calculated following Bird’s algorithm (1994). The collisions are then described using the universal potential (Ziegler *et al.* 1985), and the new velocity vectors of the ejected particles are deduced. The O atmosphere is assumed not to be changed by these collisions. A more accurate description is not warranted, since these collisions were shown to have a relatively small effect on the cloud morphology.

The position of each particle during the simulation is calculated at each time step by solving Eq. (1) with a central force

algorithm. The new position of each particle is deduced from its previous position and from the net force in Eq. (1) times the time step. The time step is chosen to be small enough to minimize the error made by solving Eq. (1) with this method. This is tested first of all by comparison with known analytical solutions of Eq. (1). At each new position of each particle, we test whether the particle reaches Europa or Jupiter or escapes the domain of the simulation. We also test the probability that each particle will be ionized, or dissociated in the case of a molecule, as described in Section 2.3.

In tracking the sodium atoms, the density of the sodium cloud is determined assuming it tends to a steady state which varies only with respect to Europa’s longitude in Jupiter’s rest frame. This requires tracking several hundred thousand test particles sputtered from Europa’s surface during 10 Europa rotations around Jupiter (which is also equal to ~ 17 times the average lifetime before ionization at Europa’s orbit). The space around Europa is divided into cells ($500 \times 60 \times 30$) which cover a sphere centered on Europa of radius $\sim 1000 R_E$. The distribution of these cells follows a height scale in order to describe the interaction of the sputtered particles with the thin atmosphere of O_2 . At each simulated rotation, Europa passes through the region corresponding to the observations of Brown (2002), that is, between ~ 109 to 122° phase angle (Table I). During this period, the time spent by every particle crossing a cell is noted and added. At the end of the simulation, the density is calculated by multiplying this value by a weight and by dividing by the volume of the cell and the total time spent by Europa in the region of the observations during the whole simulation (the number of rotations times 3 h 30 min which is the total length of the observations). The weight, w , is the number of real particles that each simulated particle represents: that is, $w = \Phi \times S_E \times T_s / n_{sim}$, where Φ is the total sputter flux, S_E is the total surface of Europa, T_s is the total time of the simulation (corresponding to the 10 Europa rotations around Jupiter), and n_{sim} is the total number of simulated particles ($\sim 10^6$). Typically, a simulated particle represents $\sim 10^{25}$ real particles. In the observation region, the integration of the column density along a line-of-sight out to $\sim 40 R_E$ from the surface requires a determination of the density out to $\sim 500 R_E$. Large distances are also needed to compare the north–south and the east–west differences. However, for the very large distances from Europa ($\sim 500 R_E$), the atom transit times (the time it takes a particle to reach such a distance) are on the order of several Europa rotations around Jupiter, so comparisons for large distances are difficult because most of the test particles have been ionized. When the integrated line-of-sight emission does not vary significantly, we assume steady state is reached.

The emission along a line-of-sight is calculated using the relative speed between each atom and the Sun. The results presented by Brown (2002) are the sum of the D1 and the D2 emission lines. Based on resonant scattering of sunlight, the ratio $D2/D1 \approx 1.66$ indicates that the emission is optically thin (Brown and Hill 1996). We use a tabulation of the emission from a Na atom vs

its speed (Brown and Yung 1976) to calculate the scattered light at the D2 line and to deduce the (D1 + D2) line's emission.

In order to test our method, we first simulated a spherical expansion by neglecting the effect of Jupiter and Europa, ionization, and solar radiation pressure. We calculated the optimized values for the time step and grid distribution with radial distance in order to reproduce the $1/r$ evolution of the integrated line-of-sight emission in such a case. The grid size close to Europa is fixed in order that the fastest particle travels more than one mean free path inside each cell below 150 km from the surface (higher than the exobase). The time step is chosen to be small enough to conserve energy and to reproduce known analytical solutions. We also reproduce the results presented in Section 3 varying the time steps, grid distribution, and number of simulated particles to optimize for accuracy and computing time.

2.3. Energy and Spatial Distribution and Ionization

Rate of the Ejecta

Since collisions with the background O_2 are few, the spatial distribution of the atoms or molecules prior to ionization is determined primarily by the initial energy distribution. The form of the initial energy distribution of the sputtered particles is guided by experiment and previous modeling. We write $f(E, \theta)$ as the probability a particle will be ejected from the surface with an energy E in a direction that makes an angle θ with the normal to the surface. This average distribution is assumed to be the same for the Na atoms and for NaX molecules (Wiens *et al.* 1997) and to be the same everywhere on Europa's surface. $f(E, \theta)$ will be described shortly.

The sputter source in Johnson (2000) was assumed to be spherically symmetric. Here a nonisotropic flux is used. The bombardment and, hence, the sputtered flux are assumed to follow a rough cosine dependence with a maximum at the apex of the trailing hemisphere, almost null values at the apex of the leading hemisphere (Popieszalska and Johnson 1989), and that is isotropic from north to south poles. Such a distribution of the bombardment is also suggested by the albedo variations. $g(\theta', \varphi')$ represents the flux of particles ejected from the surface per unit solid angle at (θ', φ') , where θ' is the latitude and φ' is the longitude. $\theta' = 0, \varphi' = 0$ is at the apex of the trailing hemisphere, whereas $\theta' = \pm \frac{\pi}{2}$ are the north and south pole positions, and $\theta' = 0, \varphi' = \pm \pi$ is the apex of the leading hemisphere. We use $g(\theta', \varphi') = \Phi/4\pi \times \cos(\varphi'/2)$ with Φ the total sputter flux. Φ is here assumed to be time independent, which we discuss in the next section.

The probability for a Na atom to be ionized or for a NaX molecule to be dissociated by electron impact depends on the local electron density and temperature. We neglect photoionization and use the 2D geometry of the electronic density in the jovian magnetosphere calculated by Bagenal (1994) allowing for the relative position of Europa to the Io torus. Extrapolating the density between contours, we calculate the probability of ionization and of dissociation in the jovian magnetosphere.

At Europa's orbit (9.4 R_J from Jupiter and a magnetic latitude between -2.9 and -4.7° in the jovian magnetospheric frame), the density ranges from 25 to 50 cm^{-3} (Bagenal 1994, Smyth and Combi 1988). This implies a lifetime for ionization of Na between 40 and 80 h at Europa's orbit (Smyth and Combi 1988) and a lifetime for dissociation of NaX between 10 and 15 h. We assume these molecules dissociate with each atom, receiving an additional energy between 0.5 and 1 eV. In this paper, we used a Na ionization lifetime at Europa's and at Io's orbits of 50 and 2 h, respectively, and a NaX dissociation lifetime of 10 and 0.4 h. The dependence of these lifetimes with respect to the distance to Io torus is calculated using the lifetimes at Europa and Io orbits and the variation of this lifetime in the jovian magnetosphere as defined in Smyth and Combi (1988). We neglect the latitudinal variation of the ionization and dissociation rates due to the oscillation of the current sheet of Jupiter's magnetosphere compared to Europa's orbital plane and the tilt of Europa's orbital plane compared to the equator plane of Jupiter. Indeed, the range of variation of the ionization and dissociation lifetime at Europa's orbit is only a few percent of the average ionization and dissociation lifetimes (from the maximum to the minimum latitudes of Europa inside Jupiter's magnetosphere). We changed the average lifetime of ionization from 40 to 60 h without seeing significant variations in the results of the simulation. Therefore, an accurate description of the lifetime which would take into account Europa's latitude inside Jupiter's magnetosphere is not warranted. At each time step and for each test particle, the probability that the particle will be ionized, or dissociated in the case of a molecule, is equal to the time step divided by the local ionization or dissociation lifetime. A random number is then computed and compared to this probability. When this random number is smaller than the probability value, the particle is assumed to be ionized and is suppressed.

The calculated sodium emission depends on the source distribution, the intensity of the source, the variation of this intensity across Europa's surface, and the energy distribution of the ejecta. These are constrained by comparing calculated emission intensity profiles to measured profiles below.

3. RESULTS

In Figs. 2a and 2b, we display the number density of the cloud of sodium around Europa in the planes (xy) and (yz) , respectively, when Europa is at a 90° phase angle. This was obtained using an energy distribution $f(E, \theta)$ defined as displayed in Table II. In addition to background sodium from Io, two energy regimes are needed to reproduce the measurements of Brown (2002). The energy, U_{lim} , is used to divide $f(E, \theta)$ into fast and slow ejecta, as discussed below.

The shape of the cloud of sodium is similar to Smyth's (1983) for Io. Figure 2a shows the asymmetry of the cloud around Europa primarily due to the combined effects of Jupiter and Europa. We also plotted three lines (solid lines with arrows) which indicate the direction and the domain of the observations

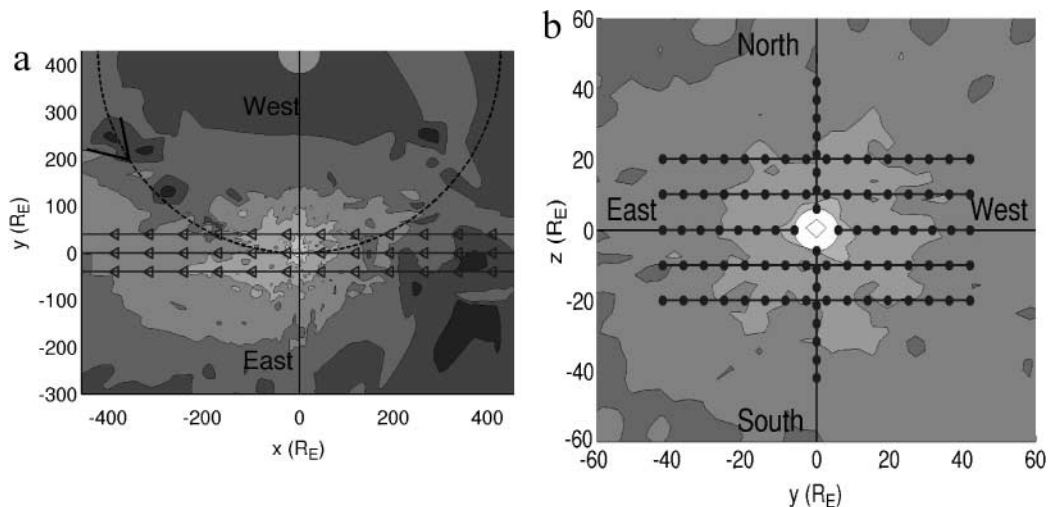


FIG. 2. Cut centered on Europa of the sodium cloud at a phase angle of 90° along. (a) Europa orbital plane. Jupiter is represented by the circle on the axis $x = 0$. Gray colors correspond to density varying by factors of 10^{-1} , from $10^{-1} \text{ Na cm}^{-3}$ (clear gray) close to Europa to $10^{-6} \text{ Na cm}^{-3}$ (dark gray) far from Europa. (b) A plane perpendicular to Europa’s orbit plane ($x = 0$). Gray colors correspond to density varying by factors of 10^{-1} , from 10^0 Na cm^{-3} (clear gray) close to Europa to $10^{-3} \text{ Na cm}^{-3}$ (dark gray) far from Europa. Also represented are the six different lines of scan made during the measurement. The energy distribution of the sputtered Na particles is the one displayed in Table II.

(Brown 2002). Figure 2b shows the asymmetry in a plane perpendicular to Europa’s orbit plane. We also show six lines (dotted lines) indicating the scans along a north–south axis (vertical line) and along an east–west axis (horizontal lines) at -20 , -10 , 0 , 10 , and $20 R_E$ from Europa. From the cloud morphology, any measurement of the column density made simultaneously on a north–south axis and on an east–west axis is more extended in the east–west direction (parallel to the y axis in Fig. 2b). This difference is due to the combined effect of the centrifugal force and the gravity of Jupiter, which has a significant effect at high latitudes.

The emission profiles along the lines shown in Fig. 2 are displayed in Figs. 3 and 4. Also given are the calculated profiles discussed below. By adjusting parameters in the calculated profiles to fit the measured profiles, we roughly characterize the sodium source (Table II). The observations given in Figs. 3 and 4 are used as follows. The integrated intensity at the closest distances to the surface, $\sim 6 R_E$, for the north–south (Fig. 3a) and east–west (Fig. 3b) primarily constrains the net surface flux Φ and the nonisotropic nature of the ejecta. In all of these figures, the decrease in intensity with respect to the distance from Europa for scans between 6 and $30 R_E$ primarily constrains the principal lower energy component in Table II of the energy distribution of the sodium sputtered from Europa’s surface. Finally, the de-

pendence of the intensity above $30 R_E$ from the surface (that is, the decrease of the emission with respect to distance) is used to roughly constrain the energetic tail of the energy distribution and the “background” sodium. Sample comparisons between observations and simulations made using different sets of parameters are shown in Figs. 5 and 6 and are described below. The source parameters obtained in this manner are given in Table II and are discussed below. In general, the integrated emission intensity calculated out of Europa’s orbital plane is noisier than in the orbital plane because of smaller statistics. Indeed, the ejected particles tend to remain close to the orbital plane because of the combined effect of the gravitational forces of Europa and Jupiter. The size of the sodium source derived from this work is based primarily on the measurements shown in Fig. 3. The measurements shown in Fig. 4 have been mainly used to constrain the background and energetic tail distribution but also as an indication of the temporal variations of the sodium cloud (Section 3.2.2).

The best simultaneous fit of the first few points in Fig. 3 at $6 R_E$ on the east–west and north–south axes are for a roughly uniform flux going from north to south poles as described in Section 2.3 (Popieszalska and Johnson 1989). The nonuniform leading/trailing flux predicted by these authors does not play a significant role. Measurements closer to the surface will be needed in order to check this dependence. In the results shown in this paper, we have used the distribution suggested by Popieszalska and Johnson (1989).

3.1. Energy Distribution: Near Europa

Laboratory measurements of the energy distribution of the ejecta in sputtering are often parametrized using $f(E, \theta) = 2EU/(E + U)^3 \times 2 \cos \theta$, where U is a parameter related to the

TABLE II

$U_{lim} = 0.8 \text{ eV}$	$f(E, \theta)$	U or U'
$E < U_{lim}$	$2EU/(E + U)^3 \times 2 \cos \theta$	$U = 0.055 \text{ eV}$
$E > U_{lim}$	$\frac{4}{9} EU^{1/3}/(E + U')^{7/3} \times 2 \cos \theta$	$U' = 0.55 \text{ eV}$

Note. E is the energy of the ejected particle and θ is the angle between its velocity and the normal to the surface.

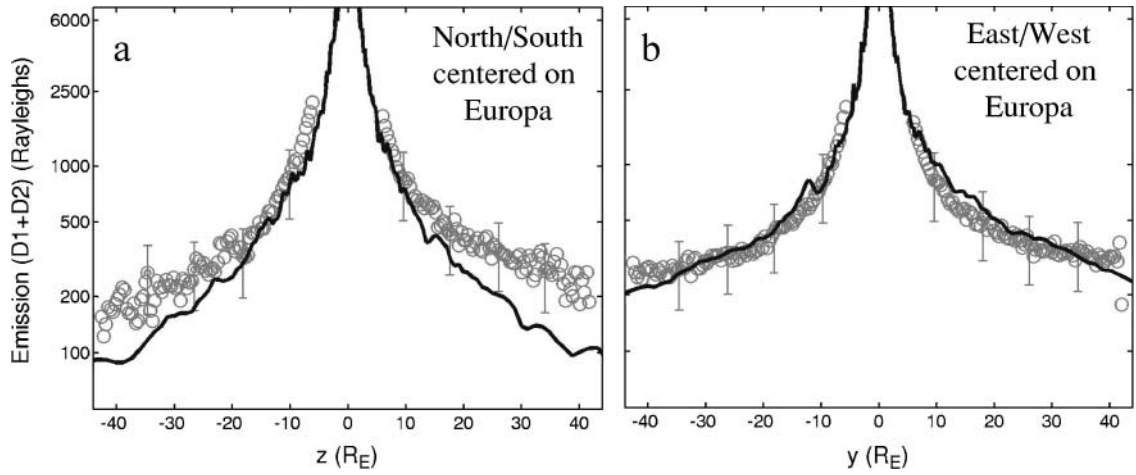


FIG. 3. Emission intensities in Rayleighs. (a) Scan centered on Europa along north–south axis (set of scan 1). (b) Scan centered on Europa along east–west axis (set of scan 2). Solid line: Simulated emission intensities integrated along x -axis for Europa at a phase angle of 90° and for an energy distribution of the sputtered Na particles as displayed Table II. Circles: Brown’s (2002) observations. Error bars correspond to overall calibration error.

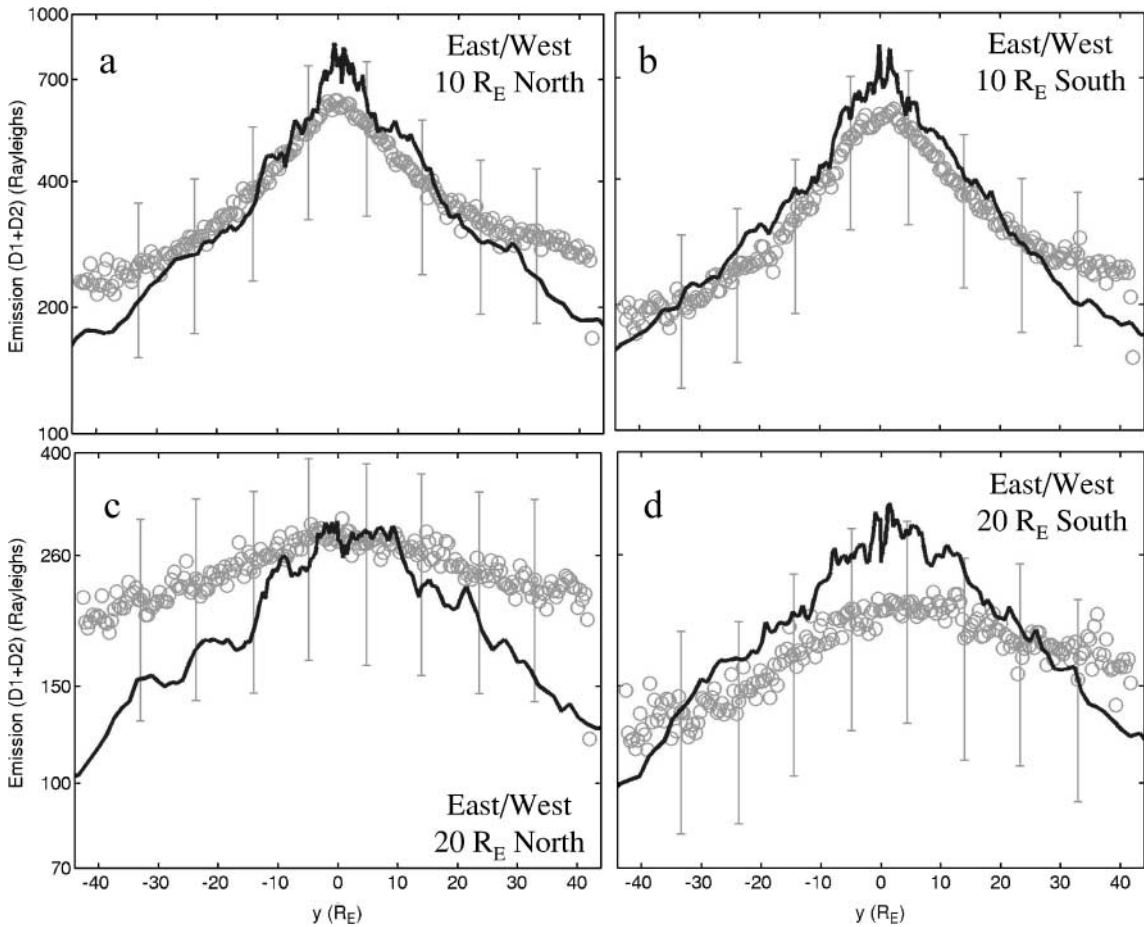


FIG. 4. Emission intensities in Rayleighs. Same symbols as in Fig. 3. Scans along east–west axis in a plane at (a) $10 R_E$ in the north (set of scan 3), (b) $10 R_E$ in the south (set of scan 4), (c) $20 R_E$ in the north (set of scan 5), and (d) $20 R_E$ in the south (set of scan 6). Error bars correspond to overall calibration error.

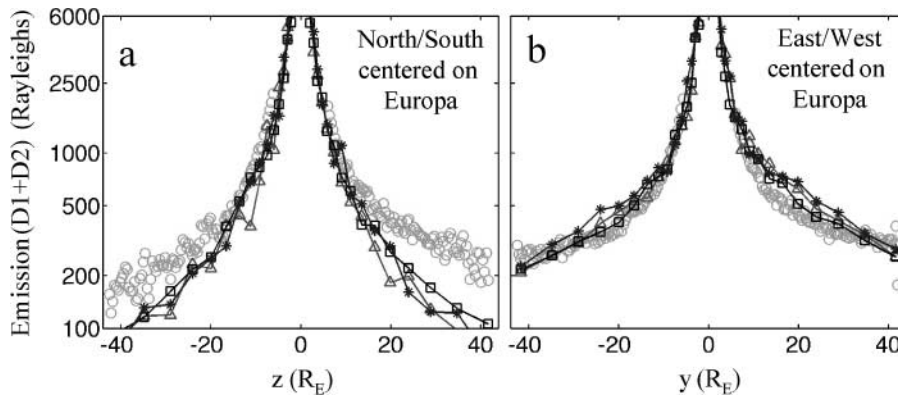


FIG. 5. Emission intensities in Rayleighs. (a) Scan centered on Europa along north–south axis (set of scan 1). (b) Scan centered on Europa along east–west axis (set of scan 2). Circles: Brown’s (2002) observations. Simulated emission intensities for Europa at a phase angle of 90° and using an energy distribution for the ejecta $f(E, \theta) = 2EU/(E + U)^3 \times 2 \cos \theta$ with $U = 0.02$ eV (solid triangle line), $U = 0.055$ eV (solid square line), and $U = 0.1$ eV (solid star line). Error bars correspond to overall calibration error.

barrier for escape from the solid. We use this form, varying the net flux and U to obtain a best fit to the data in Fig. 3. Wiens *et al.* (1997) measured sputtering of Na from solid NaSO_4 and found $U = 0.27$ eV. Johnson (2000) suggested that $U = 0.055$ eV would correspond to the sputtering of Na in an ice matrix (Reimann *et al.* 1984). Low values of U are also more likely as sputtering from a porous regolith (vs from a laboratory surface) preferentially affects the low-energy end of the spectrum (Hapke 1986). Therefore, we tested several values of U (0.01 to 0.5 eV) as sodium may be primarily sputtered from a hydrated salt or an ice-rich region, and the surface is a regolith. In Fig. 5, measured emission brightnesses are compared to simulations for $U = 0.02$, 0.055, and 0.10 eV (triangle, square, and star solid lines, respectively), adjusting the size of the flux for a best fit in each case. In Fig. 5, we did not indicate the systematic calibration errors because our purpose is to find the best fit to the decrease in emission with respect to distance. Here we consider measurements and simulations along the north–south and east–west axes and centered on Europa (as in Fig. 3). Fig. 5 shows that the emission brightness profile obtained for $U = 0.055$ eV (square line) displays the best agreement with measurements (circles), whereas emission brightness profiles obtained for larger (star) or smaller (triangle) values of U display larger discrepancies with measurements (especially for the east–west axis in Fig. 5b; for $y > 0$ that is towards Jupiter and along the north–south axis in Fig. 5a at large z values). We used $U = 0.055$ eV to obtain the profiles in Figs. 3 and 4, although changing this between ~ 0.03 eV and ~ 0.08 eV gives equally good fits within the noise of the data. The observations in Figs. 3 and 4, however, suggest the need for an even more energetic tail than that defined in Table II, and the presence of a background component.

3.2. Distant Sodium

3.2.1. Energetic tail. The comparison between simulations and observations (in particular Fig. 3a for $z > 15 R_E$) suggests

that the observed sodium cloud can be roughly separated into two components. One component populates the region close to Europa (less than $20 R_E$) and the regions beyond $20 R_E$ are populated by more energetic ejecta. The comparison between simulations and observations (between 10 to $40 R_E$) is better if the energy distribution of the sputtered Na has a slowly decreasing, high-energy component. Such a tail occurs for physical sputtering by the corotating ions and for electronically induced sputtering when the excitation density in the material is high (e.g., Johnson 1990). The latter is the case for energetic (tens of keV to MeV) O^+ and S^+ , the dominant sputtering agents at Europa (Cooper *et al.* 2001). However, the energy distributions for both physical sputtering and electronic sputtering decrease more rapidly than the energy distribution for knock-on sputtering from the atmosphere (Smyth and Combi 1997).

Profiles using two forms for the energetic tail of the distribution of the sputtered particles are compared in Fig. 6 to the observations along the north–south axis (Fig. 6a) and along the east–west axis (Fig. 6b), both centered on Europa (same as Fig. 3). The triangle solid lines correspond to the distribution $f(E, \theta) = 2EU/(E + U)^3 \times 2 \cos \theta$ with $U = 0.055$ eV having at high energy an E^{-2} dependence and normalized to the intensities near Europa. It is seen in Fig. 6 that this distribution results in somewhat lower emission intensity than that measured along the north–south axis beyond $20 R_E$ from Europa and greater emission intensity along the east–west axis between 10 to $25 R_E$ from Europa. The square solid lines in Fig. 6 have been obtained using the same distribution for energies $E < U_{lim}$ but a more energetic tail for $E > U_{lim}$, $f(E, \theta) = \frac{4}{9}EU'^{1/3}/(E + U')^{7/3} \times 2 \cos \theta$, where we used $U' = 0.55$ eV and $U_{lim} = 0.8$ eV. This distribution has been suggested by atmospheric sputtering (Smyth and Combi 1997, Johnson 2000). The fit is not excellent but is improved with the more energetic tail. The profile is not very sensitive to the choice of the energy threshold U_{lim} or of U' . However, if we had used a lower or higher U value in $f(E, \theta)$, the need for an energetic tail would have been enhanced (see

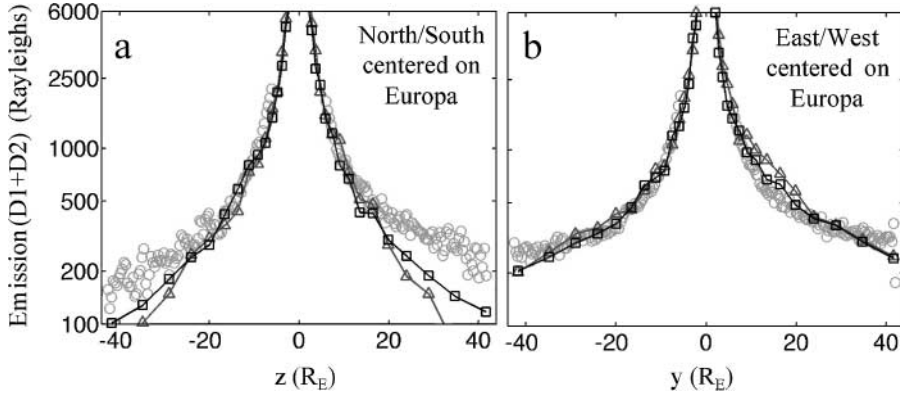


FIG. 6. Emission intensities in Rayleighs. (a) Scan centered on Europa along north–south axis (set of scan 1). (b) Scan centered on Europa along east–west axis (set of scan 2). Circles: Brown’s (2002) observations. Solid triangle line: simulated emission intensities integrated along x -axis for Europa at a phase angle of 90° and using an energy distribution of the ejecta $f(E, \theta) = 2EU/(E + U)^3 \times 2 \cos \theta$ with $U = 0.055$ eV. Solid square line: simulated emission intensities for the same conditions, with the same energy distribution for $E < U_{lim}$ and for $E > U_{lim}$ with an energetic tail that is $f(E, \theta) = \frac{4}{9}EU^{1/3}/(E + U')^{7/3}$ with $U_{lim} = 0.8$ eV and $U' = 0.55$ eV. Error bars correspond to overall calibration error.

Fig. 5). The resulting energy distribution (Table II) was used in Figs. 3 and 4.

In Fig. 7, we compare the best model-derived distribution (Table II) with measured energy distributions. The best agreement requires a low value of U , consistent with the data on the sputtering of water ice by keV heavy ions, and an energetic tail. For incident fast light ions, the energy distributions are shifted to lower energies (e.g., Johnson 1990, Reimann *et al.* 1984). The low value of U suggests that Na might be carried off due to large sputtering yields for water ice (Johnson 2000).

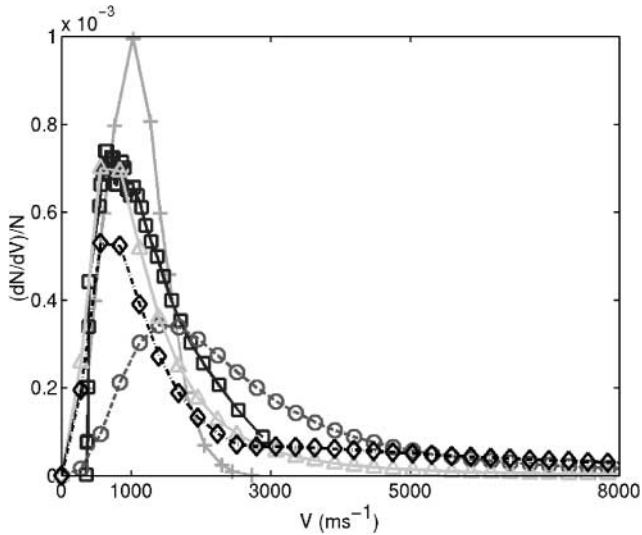


FIG. 7. Normalized energy distributions of sputtered particles. Experiment: Na from silicate (Yakshinskiy and Madey 1999) in solid line with crosses; Na from Na₂SO₄ (Wiens *et al.* 1997) in dashed line with circles; H₂O (Reimann *et al.* 1984) in solid line with triangles; Na from ice (Yakshinskiy and Madey 2002) in solid line with squares; best fit from this simulation in dashed-dotted line with diamonds with $U = 0.055$ eV, $U_{lim} = 0.8$ eV, and $U' = 0.55$ eV.

Yakshinskiy and Madey (1999) measured an energy distribution corresponding to low-energy-electron or UV-photon-stimulated desorption of sodium atoms from a lunar-like material which has a more rapidly decreasing tail than the distribution for ice sputtering. Using such a distribution in our simulations increased the discrepancies between measurement and simulation. Remarkably, the peak of the best model-derived distribution in Fig. 7, at ~ 800 m/s, appears to be in rough agreement with the measurements for sputtering of sodium from ice, which became available after this paper was submitted (solid lines with squares in Fig. 7; Yakshinskiy and Madey 2002, Johnson *et al.* 2002). Although we have used a form for atmospheric sputtering for the tail of the distribution, we presume this accounts for a number of processes which we cannot separate here: knock-on sputtering, sputtering from refractory regions, and atmospheric sputtering.

3.2.2. Background sodium and temporal variation. Assuming a background of sodium atoms can considerably improve the agreement at large distances, Wiens *et al.* (1997) found that $\sim 10\%$ of the Na that is sputtered from the surface is in a molecular form, mainly NaX. Sodium atoms from the dissociation of these sputtered molecules can have enough energy to reach the relevant distances. However, using a 10% population of NaO does not account for the background since a large fraction of the ejected molecules return to the surface before dissociating. Therefore, the background is probably not due to Na that is sputtered from Europa. Sputtering of dust grains is one possible source. Thiessenhusen *et al.* (2000) described a population of grains of 10^{-11} g with a density of 4×10^{-13} cm⁻³ at Europa’s orbit originating from Io or Europa. These grains can be sputtered by the energetic ions, producing a population of neutral Na atoms. As an example, if we assume a concentration of 1% Na (roughly what is found for Europa’s surface; see Section 3.3), a density of ~ 0.001 Na cm⁻³ can be generated by this process.

However, the main contribution to this background is Na from the Io torus region. Simulations (Smyth and Combi 1991) and measurements (Mendillo *et al.* 1990, Flynn *et al.* 1992) show an extended Iogenic sodium cloud which corresponds to an emission of 50–150 Rayleighs at Europa’s orbit. However, the background considered in this work is doppler-shifted by an amount comparable to Europa’s motion. A contribution up to ~ 100 Rayleighs ($\sim 0.008 \text{ Na cm}^{-3}$) at the doppler-shift of Europa may be possible (Smyth and Combi 1991).

Such a background would be dependent on the distances of each observation to Io’s torus and the torus plane. We arbitrarily chose a background equivalent to an emission intensity between 30 and 80 Rayleighs (which corresponds to a density between 0.002 and 0.006 Na/cm^3), which varies with respect to the distances of each observation to Io’s torus and to Io’s torus plane. The smallest background contribution (between 30 and 60 Rayleighs) is used for the observations made south to Europa (sets of scan 1 for the south part, 4 and 6) and for the east–west scan (set 2) centered on Europa. The largest (between 60 and 80 Rayleighs) is applied to the observations made north of Europa (sets 1 for the north part, 3 and 5). A larger background contribution does not significantly improve the comparison and is difficult to justify since, even ignoring the doppler-shift, 100 Rayleighs is the average Iogenic sodium emission intensity observed at Europa’s orbit (Flynn *et al.* 1992, Takahashi *et al.* 2000).

A potential variation of the source rate of sodium ejected from Europa is strongly suggested by the observations (Brown 2002). Indeed, the observations in Fig. 4 are not consistent with observations along the north–south axis shown in Fig. 3a. At $y = 0$ in Figs. 4c and 4d, an emission of 200 ± 40 Rayleighs is observed, whereas at the same location in Fig. 3a at $z = \pm 20 R_E$, the emission is 400 ± 80 Rayleighs. We observe the same discrepancy between the peaks of Figs. 4a and 4b, 600 ± 120 Rayleighs, and the corresponding point in Fig. 3a, 800 ± 160 Rayleighs. The latter discrepancy could be due to calibration error between the two sets of measurements, but for the first case, the discrepancy is larger than maximal calibration error. These differences likely correspond to temporal variations in the source rate over the time period of the measurements, $\sim 3 \text{ h } 30 \text{ min}$. They are much too large to be due only to background variations (two times the average Io’s sodium emission intensity observed at Europa’s orbit).

A large majority of the observed particles (which are the closest particles to Europa along the emission line-of-sight) have been ejected 1 to 2 h before being observed. Since the tilted dipole magnetic fields oscillate in 10 h, when the sodium reported in Fig. 3a (set 1) was ejected, Europa was in Jupiter’s current sheet near the magnetic equator (between $+0.5$ and -2° magnetic latitude). For Fig. 3b (set 2), the sodium was ejected from Europa when Europa was between -2 and -4.5° magnetic latitude; for Fig. 4a (set 3) it was between -4.5 and -6° ; for Fig. 4b (set 4), it was between -6 and -7.5° ; for Fig. 4c (set 5) it was between -7.5 and -9° ; and for Fig. 4d (set 6),

it was between -9 and -7.5° . This variation of Europa’s latitude corresponds to a variation of the distance of Europa to Io’s torus plane between 0 and $60 R_E$. From the first to the last observation, it is then probable that Europa was in a lower plasma density, so that the flux of energetic particles impacting Europa’s surface decreases in intensity during the 3 h 30 min of the observations. The flux of ejected Na particles from the surface of Europa should have changed (at least decreased in intensity) during the observations. This is in agreement with the remark made in the previous paragraph on the discrepancy between observations made at the same point but at two different times (the latest observations being less intense than the earliest).

In order to illustrate this point, we reduce the emissions obtained in Figs. 3 and 4 to reproduce the decrease of the ejected flux during the observations. Fig. 8b was obtained by reducing the emission intensity of Fig. 3b by 15%; Figs. 8c, 8d, and 8f were obtained from Figs. 4b, 4c, and 4d, respectively, by reducing the emission intensity by 25%; Fig. 8f was obtained by reducing the emission intensity of Fig. 4d by 35%. Reducing the emission intensity of the observations reported in Figs. 4a and 4b (Figs. 8c and 8d) corresponds to reducing the population of particles with enough energy to reach $10 R_E$ north or south of Europa’s orbital plane, i.e., those with initial ejecta energies $> 0.4 \text{ eV}$. For Figs. 4c and 4d (Figs. 8e and 8f), such corrections correspond to reducing the population of particles able to reach $20 R_E$ north or south of Europa’s orbital plane, i.e., those with initial energies $> 0.6 \text{ eV}$. Therefore, both the intensity *and* the energy distribution can be changing. As can be seen in Fig. 8, these corrections significantly improve the agreement between simulation and measurement, in particular when compared to the measurements in which we subtract the background (dark crosses), as described above. The results in Fig. 8 suggest one explanation of the shape of the emission brightness observed by Brown (2002). However, the systematic calibration errors place a limit on the uniqueness of this solution.

Temporal variations closer to Europa than $10 R_E$ are seen by comparing the new observations with the Brown and Hill (1996) observations, as corrected in Brown (2002). These are 20 to 100% smaller, also suggestive of a changing total source rate.

3.3. An Endogenic or Exogenic Source?

Using the results presented above, we can determine the fraction of the sputtered population on bound and escaping trajectories. By escape we mean atoms which are ionized or which reach $1000 R_E$ from Europa. For the set of parameters presented here, of the $\Phi = 3 \times 10^7 \text{ Na cm}^{-2} \text{ s}^{-1}$ sputtered from the surface, 60% return to Europa’s surface. This fraction would increase if 10% of Na is ejected as molecular NaX (Wiens *et al.* 1997). This implies that the redistribution of the Na across Europa’s surface is efficient. Of that 40% of Na atoms that escape from Europa, 28% are ionized in our study volume and 12% reach $1000 R_E$. The net flux of lost particles from Europa is $\sim 10^7 \text{ Na cm}^{-2} \text{ s}^{-1}$.

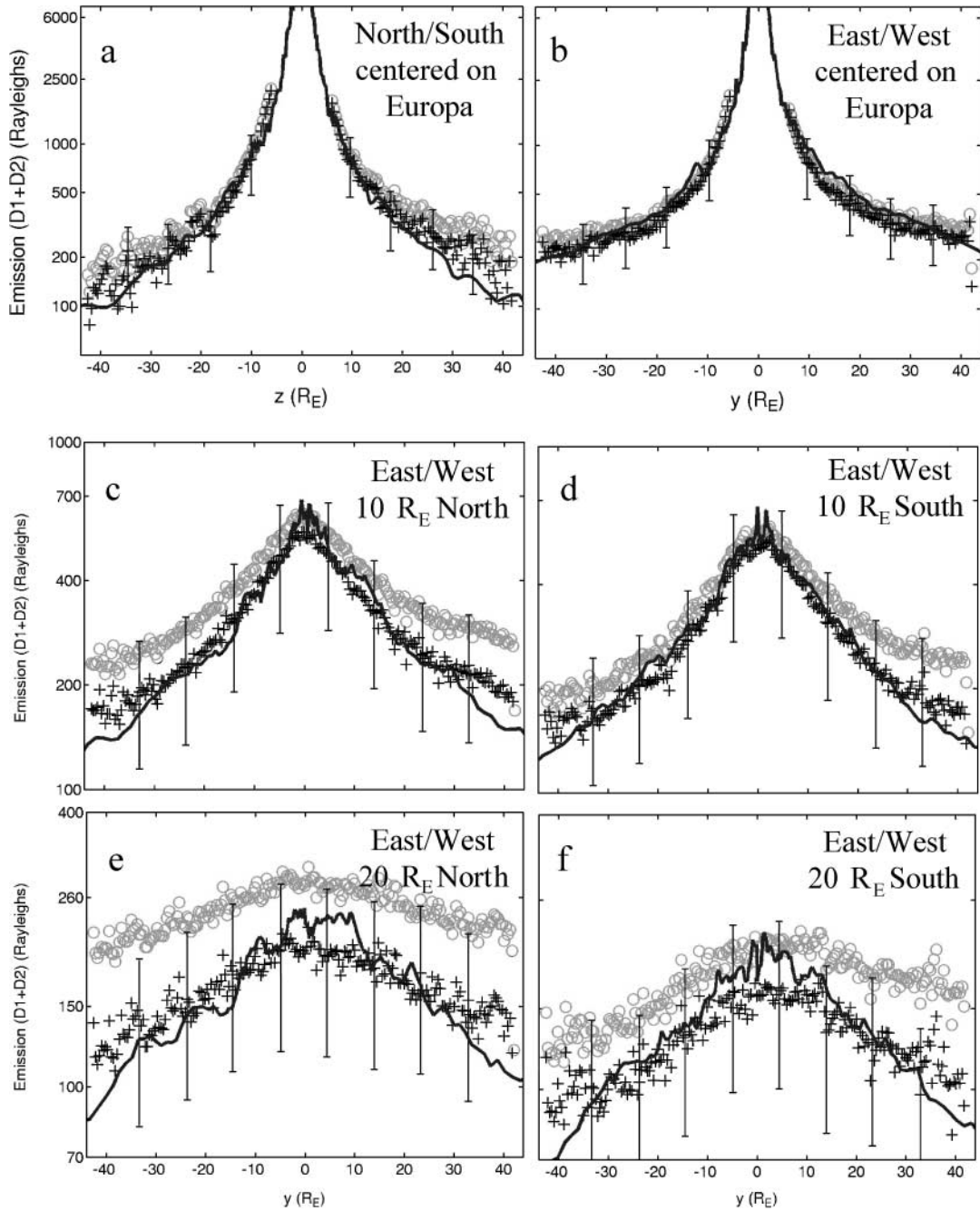


FIG. 8. Emission intensities in Rayleighs. (a) Scan centered on Europa along north–south axis with no change with respect to the results shown in Fig. 3a (solid line). (b) Scan centered on Europa along north–south axis with a 15% smaller emission intensity than shown in Fig. 3b (solid line). (c) Scan along east–west axis at $10 R_E$ in the north with a 25% smaller emission intensity than shown in Fig. 4a (solid line). (d) Scan along east–west axis at $10 R_E$ in the south with a 25% smaller emission intensity than shown in Fig. 4b (solid line). (e) Scan along east–west axis at $20 R_E$ in the north with a 25% smaller emission intensity than shown in Fig. 4c (solid line). (f) Scan along east–west axis at $20 R_E$ in the south with a 35% smaller emission intensity than shown in Fig. 4d (solid line). Circles: Brown’s (2002) observations. Solid line: simulated emission intensities integrated along x -axis for Europa at a phase angle of 90° and for an energy distribution of the sputtered Na particles as displayed in Table II. Crosses: Brown’s (2002) observations minus the background defined in Section 3.2.2. Error bars correspond to overall calibration error.

The estimate of $\sim 10^7 \text{ Na cm}^{-2} \text{ s}^{-1}$ is based mainly on the measurements and fit provided in Figs. 3a and 3b. The four sets of measurements in Fig. 4, obtained apparently for different conditions of ejecta flux and/or background than those in Fig. 3,

suggest up to $\sim 35\%$ lower flux for the fast ejecta depending on the actual background. That is, a reduction of the population with initial energy $> 0.4 \text{ eV}$. The low-energy part of the ejecta, which is $\sim 70\%$ of the ejecta, is not as strongly affected. However,

the differences between the observations reported in Brown (2002) and in Brown and Hill (1996) relate to the whole energy distribution and suggest that the total loss rate can decrease by a factor of 2. Therefore, the net loss rate from Europa is ~ 5 to $10 \times 10^6 \text{ Na cm}^{-2} \text{ s}^{-1}$.

Even allowing for these uncertainties, the net loss rate is larger than the estimate made by Johnson (2000), $2\text{--}4 \times 10^6 \text{ Na cm}^{-2} \text{ s}^{-1}$ using Brown and Hill (1996). The net loss rate found here, $\sim 5\text{--}10 \times 10^6 \text{ Na cm}^{-2} \text{ s}^{-1}$, is about one order of magnitude larger than the implantation rate for Iogenic sodium, $0.2\text{--}0.8 \times 10^6 \text{ Na cm}^{-2} \text{ s}^{-1}$, estimated in Johnson (2000). Therefore, it appears that Europa is losing much more sodium than is implanted from Io.

Based on the above, the ejected sodium is either endogenic or supplied by another exogenic source such as micrometeorites. Using an atomic concentration of $\sim 2\%$ Na, micrometeorites supply $< \sim 10^5 \text{ Na cm}^{-2} \text{ s}^{-1}$ to the leading hemisphere (e.g., Cooper *et al.* 2001), much less than that required. Therefore, the ultimate source of sodium is likely to be endogenic. Cooper *et al.* (2001) estimated the *average* flux of ions of energies $> 10 \text{ keV}$ sputtering from Europa's surface to be $\sim 2 \times 10^8 \text{ ions cm}^{-2} \text{ s}^{-1}$. In addition, lower energy ions impact the surface but with a net sputtering rate smaller than that for the fast ions (Ip *et al.* 1998), and a significant fraction of this flux may be deflected by the induced fields (Saur *et al.* 1998). Therefore, a lower bound to the required yield, that is, the ratio between the total sputter flux at the surface ($\Phi = 3 \times 10^7 \text{ Na cm}^{-2} \text{ s}^{-1}$) and the incident flux, is $\sim 0.15 \text{ Na/ion}$ incident. Using the relation between yield and concentration of Na in ice given by Johnson (2000): $Y \sim 20 C_{\text{Na}}$ implies the present Na concentration in Europa's surface would be $C_{\text{Na}} \sim 0.008$, somewhat larger than the estimate made by Johnson (2000) but sensitive to the actual flux and better measurements of the sputtering yield. For comparison, Smyth and Combi (1997) estimated a Na loss rate from Io as being equal to $2.0 \times 10^8 \text{ Na cm}^{-2} \text{ s}^{-1}$. The net loss rate of sodium given above is small geologically. Approximately 10 m of Europa's surface materials would be fully depleted in sodium in 10^9 years using an initial concentration of 1%. Maintaining Na in the penetration layer of the energetic ions and electrons ($\sim 1 \text{ cm}$) requires replenishment of this layer in $< \sim 10^6$ years.

4. CONCLUSIONS

The discovery measurements of Brown and Hill (1996) gave the first profile of the cloud of Na around Europa. Although the surface of Europa is the immediate source of the observed atmosphere, Brown and Hill (1996) concluded that the ultimate source of Europa's Na was implantation of sodium from Io. A subsequent analysis indicated that the sodium loss rate is larger than the present implantation rate (Johnson 2000), and Brown (2001) observed that the K/Na ratio at Europa differed significantly from that at Io. These papers both suggested that the sputtered sodium is predominantly endogenic. Although the implantation rate is variable and could have been much larger in

an earlier epoch, the sputtering rate would also have been larger, making a significant accumulation of Iogenic Na unlikely.

The initial measurements of Brown and Hill (1996) were recently corrected and presented along with a more complete set of measurements (Brown 2002) which are analyzed in this paper. These measurements give more detail and clearly show that the cloud is asymmetric with column vs distance from Europa differing in direction perpendicular to the orbit plane from the direction parallel to the orbit plane. Whereas Johnson (2000) used a 1D analytic model, these data required a full simulation. Here we developed a 3D Monte Carlo simulation to describe the formation of the Na cloud by sputtering of Europa's surface. In this way, we better constrain the parameters that characterize the sputtering of sodium from Europa.

We find that the dense regions of the cloud close to Europa require an energy distribution that is shifted to lower energies than that measured by Wiens *et al.* (1997) for Na sputtered from Na_2SO_4 . This is not surprising for a number of reasons. First, if the sodium exists as a sulfate or carbonate, it is in a hydrated form which is less refractory (McCord *et al.* 2001). More importantly, a large fraction of the sputtered sodium returns to the surface and is adsorbed in icy regions. Therefore, the Na atoms are likely to have an energy spectrum closer to that associated with the large sputtering yields for ice (Johnson 2000). The peak in the energy distribution used here to fit the observation is consistent with electronic sputtering from an ice surface (Reimann *et al.* 1984, Yakshinskiy and Madey 2002), and the distribution is remarkably consistent with laboratory measurements that became available after the submission of this manuscript (Johnson *et al.* 2002) and support our analysis.

Modeling the more distant sodium is problematic due to the very long flight times of the atoms, the systematic calibration error bars, and the length of the observation time for the complete set of scans. Ignoring these uncertainties, we give a rough fit of the distant sodium cloud. This component appears to have a "background," which is likely to be Iogenic sodium moving at speeds consistent with the doppler shift for Europa sodium or sodium sputtered from grains. In addition, the surface source rate appears to be variable (up to a factor of 2 for the energetic part of the ejected Na population) implying a variability in the composition of the flux of the jovian plasma to Europa's surface. Finally, the source distribution appears to require an energetic tail that is sensitive to the choice of background. It can be due to sputtering from the more refractory regions as discussed but appears closer to the form found by Smyth and Combi (1997) for Na sputtered from Io's atmosphere, although such a process alone cannot account for the flux required.

Based on the model shown in Fig. 2, we can estimate the atmospheric density of Na atoms near Europa's surface, 900 Na cm^{-3} , $\sim 10^5$ less than the O_2 atmosphere. This is larger than the early estimate of Brown and Hill (1996) but in reasonable agreement with Johnson (2000). The loss of sodium atoms from Europa is found here to be $\sim 5\text{--}10 \times 10^6 \text{ cm}^{-2} \text{ s}^{-1}$ depending on the time variability of the ejecta flux. This is about one order of magnitude

larger than the estimate of the Iogenic implantation rate. Therefore, either another exogenic source, such as micrometeorites or grains from Io, is required or the sodium is endogenic. Since the supply rate by micrometeorites is too small, we suggest that the sputtered sodium is most likely endogenic, although additional observations and modeling are needed to strengthen this important result. Here we estimate that this source must provide a net flux of $\sim 4\text{--}9 \times 10^6 \text{ Na cm}^{-2} \text{ s}^{-1}$ at Europa's surface.

Although sputtering occurs from all regions on Europa's surface, the ultimate source of endogenic sodium must be regions having a young surface. Since such regions are associated with upwelling of subsurface material (Pappalardo *et al.* 1999), the observed sodium may come from the decomposition of hydrated salts (Johnson 2001), or other minerals, originally from Europa's putative subsurface ocean. This should encourage observers to look for gas-phase ejecta indicative of other species from this ocean, including organics and, possibly, biomolecules (Johnson *et al.* 1998).

ACKNOWLEDGMENTS

The work at Virginia was supported by the NSF Astronomy Division and by NASA's Planetary Atmospheres Program.

REFERENCES

- Bagenal, F. 1994. Empirical model of the Io plasma torus: Voyager measurements. *J. Geophys. Res.* **99**, 11,043–11,062.
- Bass, D., and R. E. Johnson 2001. *Europa ocean chemistry and surface sputtering influences*. *Europa Workshop, Feb. 1–2, Ames, Moffett Field, CA*.
- Bird, G. A. 1994. *Molecular Gas Dynamics and the Direct Simulation of Gas Flows*. Clarendon, Oxford.
- Brown, M. E. 2001. Potassium in Europa's atmosphere. *Icarus* **151**, 190–195.
- Brown, M. E. 2002. The structure and variability of Europa's sodium atmosphere. *Icarus*, submitted.
- Brown, M. E., and R. E. Hill 1996. Discovery of an extended sodium atmosphere around Europa. *Nature* **380**, 229–231.
- Brown, R. A., and Y. L. Yung 1976. Io, its atmosphere and optical emissions. In *Jupiter* (T. Gehrels, Ed.), pp. 1102–1145. Univ. of Arizona Press, Tucson.
- Carlson, R. W., and 13 colleagues 1999. Hydrogen peroxide on the surface of Europa. *Science* **283**, 2062.
- Chrisey, D. B., R. E. Johnson, J. W. Boring, and J. A. Phipps 1988. Ejection of sodium from sodium sulfide by the sputtering of the surface of Io. *Icarus* **75**, 233–244.
- Cooper, J. H., R. E. Johnson, B. H. Mauk, and N. Gehrels 2001. Energetic ion and electron irradiation of the icy Galilean satellites. *Icarus* **149**, 133–159.
- Flynn, B., M. Mendillo, and J. Baumgardner 1992. Observations and modeling of the jovian remote neutral sodium emissions. *Icarus* **99**, 115–130.
- Hall, D. T., D. F. Strobel, P. D. Feldman, M. A. McGrath, and H. A. Weaver 1995. Detection of an oxygen atmosphere on Jupiter's moon Europa. *Nature* **373**, 677.
- Hapke, B. 1986. On the sputter alteration of regoliths of the outer Solar System bodies. *Icarus* **66**, 270–279.
- Ip, W.-H., D. J. Williams, R. W. McEntire, and B. H. Mauk 1998. Ion sputtering and surface erosion at Europa. *Geophys. Res. Lett.* **25**, 829.
- Johnson, R. E. 1990. *Energetic Charged-Particle Interactions with Atmospheres and Surfaces*. Springer-Verlag, Berlin.
- Johnson, R. E. 2000. Sodium at Europa. *Icarus* **143**, 429–433.
- Johnson, R. E. 2001. Surface chemistry in the Jovian magnetosphere radiation environment. In *Chemical Dynamics in Extreme Environments* (R. Dessler, Ed.), Advanced Series in Physical Chemistry **11**, Ch. 8, 390–419. World Scientific, Singapore.
- Johnson, R. E., L. J. Lanzerotti, and W. L. Brown 1982. Planetary applications of ion induced erosion of condensed gas frosts. *Nucl. Instrum. Methods* **198**, 147–158.
- Johnson, R. E., R. M. Killen, J. H. Waite, and W. S. Lewis 1998. Europa's surface and sputter-produced ionosphere. *Geophys. Res. Lett.* **25**, 3257–3260.
- Johnson, R. E., F. Leblanc, B. V. Yakshinskiy, and T. E. Madey 2002. Energy distribution for desorption of sodium and potassium from Ice: The Na/K ratio at Europa. *Icarus* **156**, 136–142.
- Khurana, K. K., M. G. Kivelson, D. J. Stevenson, G. Schubert, C. T. Russell, R. J. Walker, and C. Polansky 1998. Induced magnetic fields as evidence for substance oceans in Europa and Callisto. *Nature* **395**, 777.
- Kivelson, M. G., K. K. Khurana, D. J. Stevenson, L. Bennett, S. Joy, C. T. Russell, R. J. Walker, C. Zimmer, and C. Polansky 1999. Europa and Callisto: Induced or intrinsic fields in a periodically varying plasma environment. *J. Geophys. Res.* **104**, 4609–4626.
- Kivelson, M. G., K. K. Khurana, C. T. Russell, M. Volwerk, R. J. Walker, and C. Zimmer 2000. Galileo magnetometer measurements: A stronger case for a subsurface ocean at Europa. *Science* **289**, 1340–1343.
- McCord, T. B., T. M. Orlando, G. Teeter, G. B. Hansen, M. T. Sieger, N. G. Petrik, and L. Van Keulen 2001. Thermal and radiation stability of the hydrated salt minerals epsomite and natron under Europa environmental conditions. *J. Geophys. Res.* **106**, 3311–3319.
- Mendillo, M., J. Baumgardner, B. Flynn, and W. J. Hughes 1990. The extended sodium nebula of Jupiter. *Nature* **348**, 312–314.
- National Research Council 1998. *A Science Strategy for the Exploration of Europa*. Natl. Acad.–Natl. Res. Council, Washington, DC.
- Pappalardo, R. T., and 13 colleagues 1999. Does Europa have a subsurface ocean? *J. Geophys. Res.* **104**, 24,015–24,056.
- Paranicas, C., R. W. McEntire, A. F. Cheng, A. Lung, and D. J. Williams 2000. Energetic charged particles near Europa. *J. Geophys. Res.* **105**, 16,005–16,015.
- Popieszalska, M. K., and R. E. Johnson 1989. Magnetospheric ion bombardment profiles of satellites: Europa and Dione. *Icarus* **78**, 1–13.
- Reimann, C. T., J. W. Boring, R. E. Johnson, J. W. Garrett, and K. R. Farmer 1984. Ion-induced molecular ejection from D₂O ice surface. *Science* **147**, 227–240.
- Saur, J., D. F. Strobel, and F. M. Neubauer 1998. Interaction of the Jovian magnetosphere with Europa: Constraints on the neutral atmosphere. *J. Geophys. Res.* **103**, 19,947–19,962.
- Smyth, W. H. 1979. Io's sodium cloud: Explanation of the East–West asymmetries. *Astrophys. J.* **234**, 1148–1153.
- Smyth, W. H. 1983. Io's sodium cloud: Explanation of the East–West asymmetries II. *Astrophys. J.* **264**, 708–725.
- Smyth, W. H. 1986. Nature and variability of Mercury's sodium atmosphere. *Nature* **323**, 696–699.
- Smyth, W. H., and M. R. Combi 1987. Correlating East–West asymmetries in the jovian magnetosphere and the Io sodium cloud. *Geophys. Res. Lett.* **14**, 973–976.
- Smyth, W. H., and M. R. Combi 1988. A general model for Io's neutral gas clouds. II Application to the sodium cloud. *Astrophys. J.* **328**, 888–918.
- Smyth, W. H., and M. R. Combi 1991. The sodium zenocorona. *J. Geophys. Res.* **96**, 22,711–22,727.
- Smyth, W. H., and M. R. Combi 1997. Io's sodium corona and spatially extended cloud: A consistent flux speed distribution. *Icarus* **126**, 58–77.

- Takahashi, S., H. Misawa, H. Nozawa, A. Morioka, R. Sood, S. Okano, and K. Yumoto 2000. Distribution of sodium cloud near Io and in the inner jovian magnetosphere. *Adv. Space Res.* **26**, 1529–1532.
- Thiessenhusen, K.-U., H. Krüger, F. Spahn, and E. Grün 2000. Dust grains around Jupiter—The observations of the Galileo Dust Detector. *Icarus* **144**, 89–98.
- Westley, M. S., R. A. Baragiola, R. E. Johnson, and G. A. Baratta 1995. Ultra-violet photodesorption from water ice. *Planet. Space Sci.* **43**, 1311–1315.
- Wiens, R. C., D. S. Burnett, W. F. Calaway, C. S. Hansen, K. R. Lykkem, and M. L. Pellin 1997. Sputtering products of sodium-sulfate: Implications for Io's surface and for sodium-bearing molecules in the Io torus. *Icarus* **128**, 386–397.
- Yakshinskiy, B. V., and T. E. Madey 1999. Photon-stimulated desorption as a substantial source of sodium in the lunar atmosphere. *Nature* **400**, 642.
- Yakshinskiy, B. V., and T. E. Madey 2002. Electron and photon-stimulated desorption of K from an ice surface. *J. Geophys. Res.* **106**, 33,303–33,308.
- Ziegler, J. F., J. P. Biersak, and V. Littmark 1985. *The Stopping and Range of Ions in Solids*. Pergamon, Elmsford, NY.